

Investigation of Radial Gap Size Change under Load and the Impact on Performance for a Twin Screw Compressor using Numerical Simulation

Rainer Andres, Jan Hesse and Andreas Spille

CFX Berlin Software GmbH, Karl-Marx-Allee 90a, D-10243 Berlin, Germany

rainer.andres@cfx-berlin.de

Abstract. Computational Fluid Dynamics (CFD) and the Finite Element Method (FEM) are common and validated tools in research and industry for solving fluid flow or performing structural analysis respectively. Despite being rather challenging, also the numerical simulation of screw compressors benefits from development and enhancement of numerical models, tools and methodologies. Differences between the real machine and the numerical model are inevitable, yet increasing accuracy and prognosis quality are desired by refining existing models and accounting for specific phenomena.

Clearances within the working chamber (mainly intermesh clearance between rotors and axial and radial gaps between rotors and housing) strongly affect the flow characteristics, efficiency and thus the overall compressor performance. These clearances change under operating conditions because of thermal expansion or due to forces acting on the structure, whereas the clearance size is often only known for the reference state out of operation. The extent of deformation and the quantification of the resulting clearances is therefore of high interest in order to get the numerical model closer to real operating conditions.

In this paper numerical simulation was used to determine the change in radial gap size between rotors and housing when the compressor is running and exposed to thermal and pressure loads. For a specific operating point, a 3D-CFD simulation for a 4-6 twin screw compressor with SRM profiles was conducted for the undeformed reference compressor geometry to calculate the flow field within the machine. Also, the temperature field within the housing and rotor solids was computed using the Conjugated Heat Transfer (CHT) method. The temperature and pressure fields were then submitted to the FEM solver to compute the deformation of rotors and housing. The results of this structural analysis served as input for a modification of geometry and numerical grids to account for the change in radial gap size. A re-run of the flow simulation in the deformed state enabled to quantify the impact on the machine performance and specific flow quantities. It could be shown that taking deformation into account, the volumetric efficiency is clearly affected.

Commercial solvers from Ansys were utilized for solving fluid and structure. The spatial discretization of the fluid volume around the rotors was realized by employing pre-generated grids using the mesh generator TwinMesh. Here, the rotor deformation can be defined in dependence of the axial position. The mesh of the housing maintained unchanged for all CFD simulations as a resulting gap size was determined by considering housing and rotor deformation relative to each other.

1. Introduction

Screw compressors are widely used in the industry, e. g. for pneumatic power tools or in the automotive industry. In this paper an oil free compressor is modeled, which is often used when purity of the air is critical. Within oil injected compressors, there is the risk of contaminated air which has an adverse effect

of downstream processes and production. However, oil free compressors lack the sealing and cooling effect of the oil, thus in general the achieved pressure ratios are lower compared to oil flooded compressors. Furthermore, the lack of sealing increases leakage losses, and the lack of cooling increases solid temperatures and therefore expansion.

In the CFD simulation axial and radial clearances are fully resolved to account for gas flow between the rotors and between rotor and housing. These clearances lead to reverse flows through the gaps from the chamber with higher pressure to the one with lower pressure and therefore losses inside the machine. The initial gaps will change under operating conditions because of thermal expansion or due to forces acting on the structure. The impact on calculation results when taking the gap change into account due to thermal deformation is demonstrated in [1] and [2].

For the manufacturer, reliable tools to evaluate overall machine performance such as compression ratio and power consumption as well as to calculate losses and efficiency are of great desire. Also, the impact of design changes should be evaluated before prototypes are built so that developing costs can be reduced.

The compressor investigated in this work consists of a generic housing geometry and rotors with SRM profiles. Table 1 lists the essential parameters for the undeformed geometry.

	Male rotor	Female rotor	
Number of lobes	4	6	-
Length	168.1		mm
Tip diameter	101.9	101.1	mm
Root diameter	58.7	57.9	mm
Rotor Wrap angle	300	200	deg
Center distance	80		mm
Inner volume ratio	2.2		-

Table 1: Geometry parameters of the investigated screw compressor

2. Rotor Chamber Modeling

The rotor chambers of the screw compressor consist of volumes, which deform over time, depending on the rotor position. The chambers are connected by gaps that allow the rotation of the rotors in the static housing. Due to the intermeshing of the two rotors, the chambers strongly deform. For most CFD codes, several approaches are possible to account for this deformation. For a systematic introduction to 3D CFD simulations of screw compressors see [3]. Various methodologies for chamber modeling and the corresponding advantages and disadvantages are shown in [3]. Common approaches are e. g. automatic remeshing, immersed solid methods or customized grid generation.

The present analysis uses an automated mesh generation by the commercial software TwinMesh. At a fixed angle increment, the working chamber volumes around both rotors are discretized for the different rotor positions with a hexahedral 3D mesh consisting of two O-type grids. Here, the rotational periodicity of the rotor pair is considered, so that the set of grids is only generated for one pitch angle, i. e. 90° (360° divided by the number of male rotor lobes). This meshing approach and the CFD models were validated for a 2-stage screw compressor [5], a screw refrigeration compressor [6], and a screw expander [7], and in several confidential projects for clients.

Within the intermesh region, the two O-type grids are 1:1 connected to each other. Inflation layers near rotor and housing walls are present. Also, as part of the working chamber grid, radial, axial and intermesh clearances are taken into account. A 2D slice of the working chamber grid is shown in Figure 1.

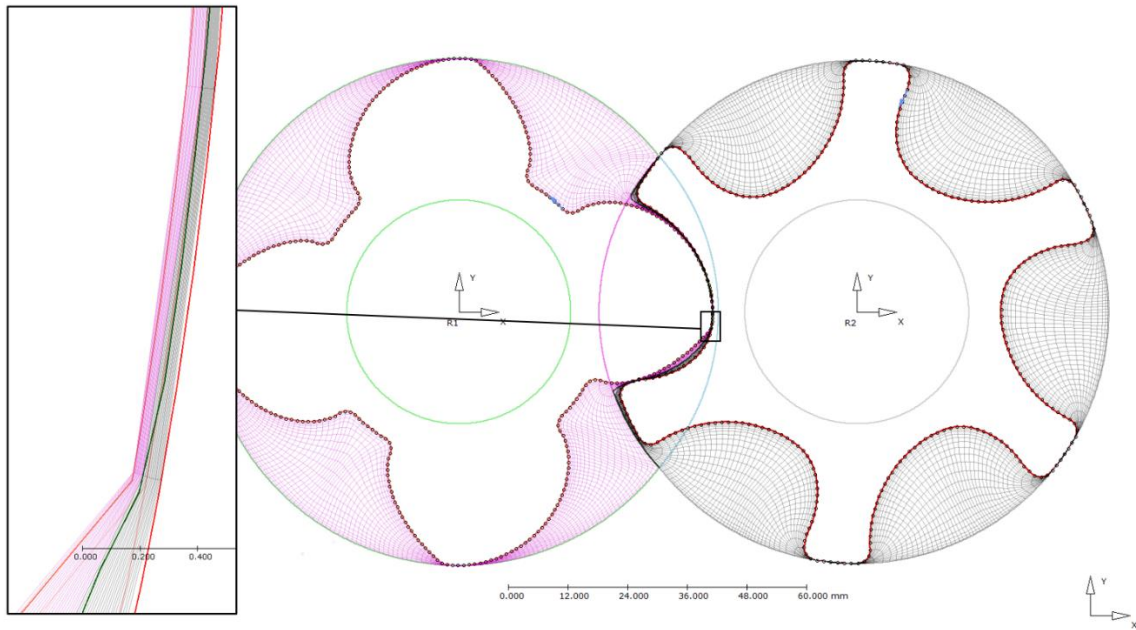


Figure 1: 2D cross section through the working chamber of the compressor

During the transient simulation, the location of each working chamber grid node is updated depending on the rotation angle via a routine at the start of each time step. The mesh topology is retained (node numbers and node connectivity), therefore no interpolation between individual time steps is necessary. An exception from this rule is the start of a new pitch angle range (i. e. every 90° of male rotation angle) because the set of pre-generated grids is re-used and results are interpolated from the last to the first grid in the set.

3. Simulation Setup

3.1. Methodology of fluid-structure interaction

The aim of this paper is to evaluate the change of the radial clearance sizes of the screw compressor due to thermal and pressure load and its effect on compressor performance. Three simulation steps are done sequentially:

1. Transient CFD simulation of the screw compressor with straight rotors and uniform radial gap size of $50\ \mu\text{m}$; conjugate heat transfer (CHT) is included to account for solid heating of rotors and housing
2. Steady-state structural simulation of rotors and housing with loads from step 1 (temperatures of rotors and housing are almost constant, pressure load is taken arbitrarily from last time step)
3. Transient CFD simulation of the screw compressor with deformed rotors; the deformation is taken from step 2; since TwinMesh does not support housing deformation (this will be included in the next release) but only shaft deflection and rotor expansion, these are chosen so that the radial gap sizes of step 2 are met best.

3.2. Fluid Setup

The simulations are set up and performed in the commercial solver Ansys CFX. Figure 2 shows the assembly of the setup which consists of separate grids for fluid and solid parts. The fluid grids discretize the working chambers and the stator volumes, the solid grids represent the solid parts for rotors and casing. Table 2 gives an overview on the mesh resolution of the different parts of the CFD simulation.

	Vertices	Elements
Fluid around male rotor	830,700	776,000 hexahedrons
Fluid around female rotor	877,500	816,000 hexahedrons
Fluid in stator	263,981	217,042 tetrahedrons; 91,719 prisms; 166,434 hexahedrons
Solid of male rotor	22,145	83,138 tetrahedrons
Solid of female rotor	23,788	88,223 tetrahedrons
Solid of casing	390,120	923,058 tetrahedrons; 263,697 prisms; 47,200 hexahedrons

Table 2: Number of vertices and elements in the meshes for the CFD simulation

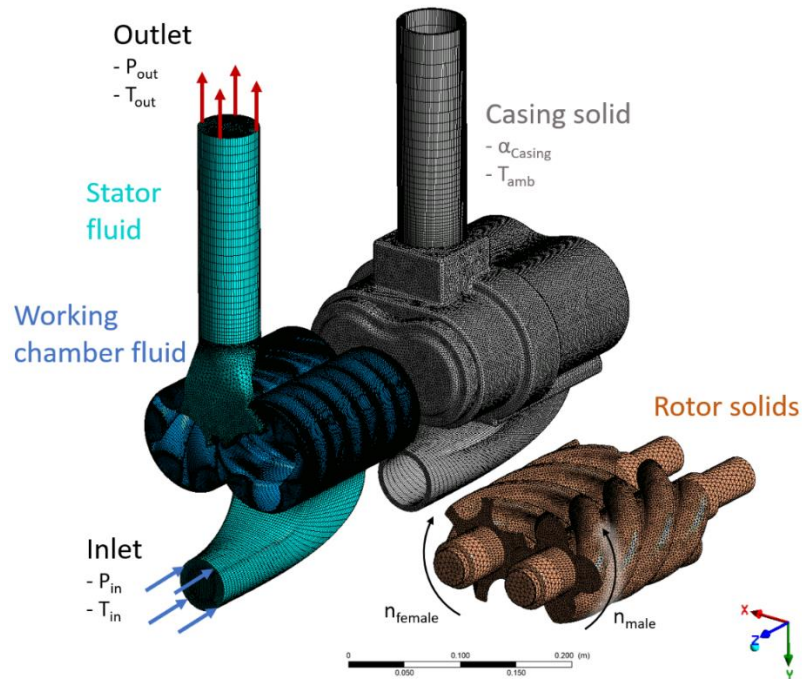


Figure 2: Boundary conditions and numerical grids for fluid and solid parts: Top right shows static solid for casing and pipe walls, bottom right the two rotating solids for the rotors; left side shows the fluid volumes consisting of static parts in suction and pressure ports and connected pipes (light blue) and deforming parts around both rotors (dark blue). The inlet is at bottom, the outlet at top side.

For the conservative flux of mass, momentum and energy between individual fluid volumes, i. e. stator volume and deforming working chamber, fluid-fluid interfaces are specified. In addition, heat flux between fluid and solids as well as temperatures within the structure are calculated using fluid-solid interfaces and the CHT method. Here, convection boundary conditions are set for the outer walls of the structure. At the outer casing wall, an ambient temperature of 20°C is assumed with an estimated heat transfer coefficient of 10 W/(m² K) for quiescent air [8]. The rotor shafts are usually located within an enclosure and experience heat dissipation from the bearings. Since these parts are not considered in the model, for the outer walls of the rotor shafts an estimated and fixed temperature of 70°C is specified.

The operating point for all calculations is defined by a rotational speed of the male rotor of 12 333 rev/min and a pressure ratio between inlet and outlet of 1:3. The fluid is air as an ideal gas, all solids are from steel. The boundary conditions are summarized in Table 3. Inlet and outlet are specified as openings via non-reflective boundary conditions; outlet temperature is only needed in case of backflow. The radial, axial and intermesh clearances for the initial run without deformation are shown in Table 4. For this investigation, synchronized rotors are considered, thus the intermesh clearance between male and female rotor is constant.

Angle increment (male rotor)	$\Delta\theta$	1	deg
Time step	Δt	13.51	μs
Rotation speed male	n_{male}	12333	rev/min
Rotation speed female	n_{female}	8222	rev/min
Inlet pressure (total)	p_{in}	1	bar(a)
Outlet pressure (static)	p_{out}	3	bar(a)
Inlet temperature	T_{in}	20	C
Outlet temperature	T_{out}	160	C
Rotor shaft temperature	T_{shaft}	70	C
Ambient temperature	T_{amb}	20	C
Heat transfer coefficient for outer casing walls	α_{casing}	10	W/(m ² K)

Table 3: Boundary conditions of the initial run

Radial male (uniform)	50	μm
Radial female (uniform)	50	μm
Axial male (equal for pressure and suction side)	100	μm
Axial female (equal for pressure and suction side)	100	μm
Intermesh	100	μm

Table 4: Clearances for the initial simulation run

As shown above, the required order of magnitude for time step to calculate the fluid field is approx. 14 μs leading to (depending on mesh resolution and used hardware) computational times in the range of hours for one revolution. Opposed to this timescale, the required time to heat up the structure is significantly larger in the range of 100,000 revolutions. Based on experience, it may take 10-15 min until the rotor and casing solids reach a certain operating temperature. It is not applicable to cover this rather large time span, so that a transient simulation of the full heating up cannot be done. Here, we are only interested in the periodic state after the heat up phase, i. e. chamber pressures and temperatures change periodically due to rotation, and solid temperatures are almost constant with only very small periodic changes. Once this temperature level is reached it is assumed that for a fixed point within the rotor or housing, the local temperature should be almost constant, independent of the rotation angle.

To overcome this challenge, the timescale for the energy equation within the solid volumes is increased by a factor up to 10,000 at simulation start so that solid temperatures increase fast. This approach is similar to decreasing the heat capacity of the solid material. Once the temperature monitors within the solids approach a periodic state, the timescale factor is decreased sequentially down to a value of 100. This reduction is necessary because the larger timescales artificially increase the fluctuation at the monitored points and lead to inhomogeneous temperature distributions, especially in circumferential direction, where the rotor lobe which lies within a pocket of hot gas heats up faster than in reality due to this acceleration approach.

The position of the temperature probes in the male rotor solid near the pressure side can be seen in Figure 3. As it can be seen in Figure 4, their temperatures show still differences between individual lobes and trends regarding the mean value; especially timescale factor 1000 should have been used for a longer time. Moreover, timescale factors lower than 100 are not considered here to limit the simulation effort required for this analysis. It must be noted that the temperature probes for the individual rotor lobes do not share the exact same radial and circumferential position, since they are only attached to the nearest grid node relative to this, whereas the mesh is not periodic in circumferential direction.

To improve these results, simulation time should be extended as well as the monitoring methodology to reduce errors introduced by these factors. Still, as a compromise between simulation time and accuracy, the outlined methodology is considered acceptable, where general feasibility of the workflow and the significance of taking deformations into account are in focus.

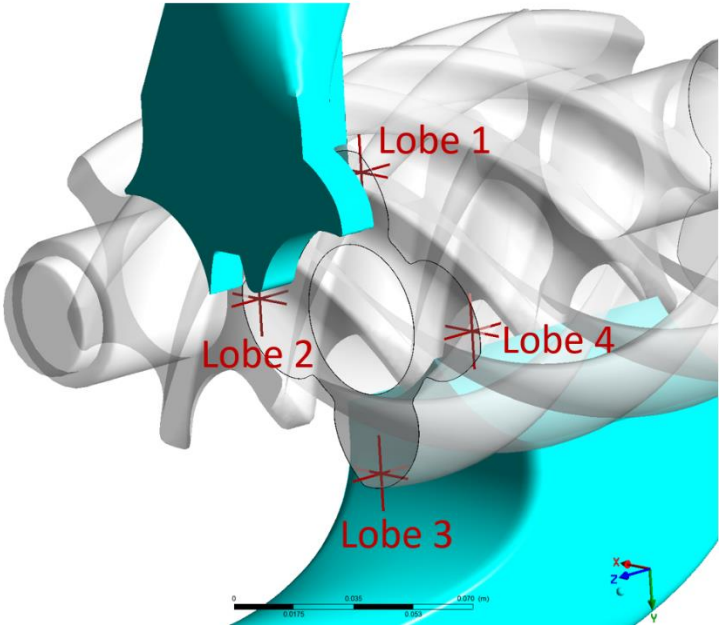


Figure 3: Temperature probes at each lobe for the male rotor

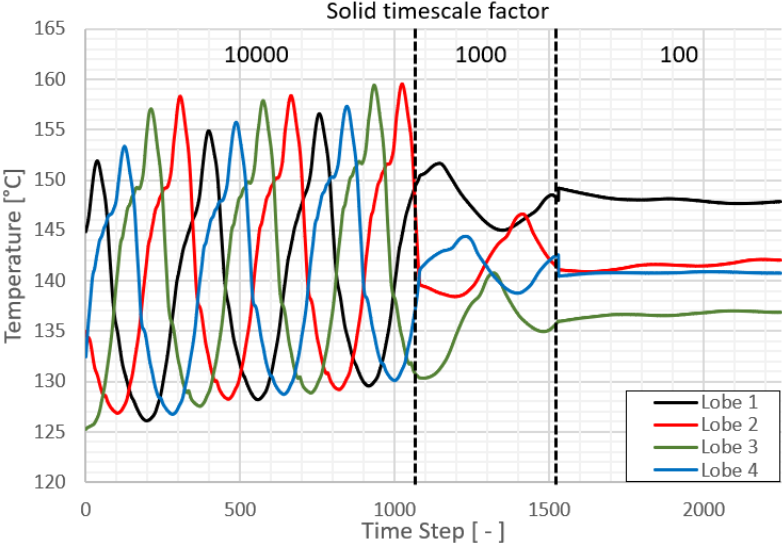


Figure 4: Temperature at male rotor probes for 3 different solid timescale factors (10000, 1000, 100)

3.3. Structural Setup

The structural simulation for the screw compressor is done in the commercial solver Ansys Mechanical (Mechanical APDL). The structural model includes the geometry of both rotors and the whole casing, from inlet to outlet. A fixed and arbitrary rotor position is used for the steady-state structural simulation. The influence of the rotational position is not investigated and might be a topic for further work.

A cut through the CAD model is shown in Figure 5, with the male rotor in blue, the female rotor in orange and the housing in green. Highest impact on the deformation of the bodies has the temperature, which leads to thermal strains from temperature gradients and overall thermal expansion. The thermal and pressure loads for the static structural simulation are taken from the last CFD time step. Due to the high heat capacity of the steel, the temperature inside the solids remains nearly constant. Any influence due to rotor dynamic effects, like gyroscopic forces and interferences due to eigenfrequencies, were neglected.

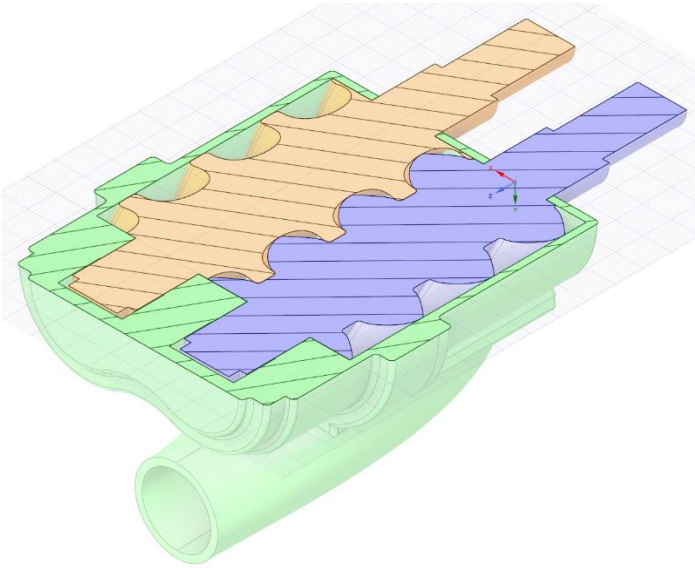


Figure 5: Cut through the CAD model with the male rotor in blue, the female rotor in orange and the housing in green

The goal is to determine the displacement of the housing and the rotors due to gravitational force, centrifugal force, operating pressure and operating temperature. From the displacements the changes in radial and axial clearances between both rotors and the rotors and the housing are derived. The structural and thermal material properties of the structural steel used for the rotors and casing are given in the following table 3.

	Steel
Density	7850 kg/m ³
Young's modulus	200 GPa
Poissons ratio	0.3
Coefficient of thermal expansion	1.2e-5/K

Table 5: Material properties of structural steel

On the left side both rotors are supported on the second shaft shoulder with a floating bearing to a fixed reference point in space (not moving), see Figure 6. This side represents the motor. On the right side on the second shaft shoulder, they are supported by a fixed bearing to the inner casing. For the fixed bearing the axial displacement is fixed, with no axial stiffness defined. This is necessary to keep the axial gap on the discharge side less depended on the thermal expansion of the rotor. For both bearings a radial stiffness of 500,000 N/mm is considered. The casing is supported on two fixed points and a frictionless support on the bottom horizontal face of the outlet, to let the housing deform as freely as possible due to temperature changes.

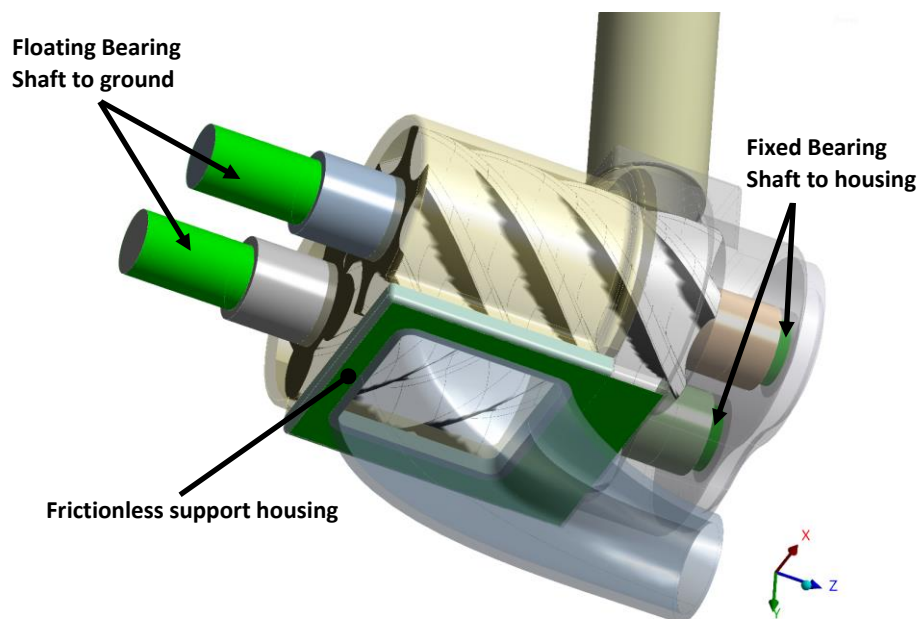


Figure 6: Bearing conditions

Between the rotating shafts and the housing no contacts are defined. The initial radial clearances are $50\ \mu\text{m}$ and the initial axial clearances are $100\ \mu\text{m}$. If contact between bodies is assumed, due to higher deformations, frictional contacts can be used. To assure a minimal clearance between both shafts or the shafts and the housing for the CFD simulation, a minimum contact distance or clearance can be defined. This minimum clearance cannot be interpenetrated.

Both the rotors and housing are meshed with Ansys Meshing. The shafts are meshed with high quality hexahedral elements. Due to the geometric complexity of the housing, it is meshed with tetrahedrons. The CFD results of the distributed pressure and the temperature on the inside of the rotors and the inner casing are interpolated on the FEM mesh, for one time step.

4. Results

4.1. CFD results for initial geometry

The screw compressor compresses the air from 1 bar to 3 bar, see pressure distribution in Figure 7.

Due to compression the temperature increases towards the discharge port, see temperature distribution in Figure 1. The figure shows the temperature on the rotor walls and on a slice plane through each rotor axis to see the temperature also in the casing solid.

Velocities are shown in Figure 9. The high velocities are located in the clearances. Depending on the pressure change and the clearance size backflow results which reduces the efficiency of the machine.

The mass flow is nearly constant at the inlet and fluctuating at the outlet depending on the size of over-compression at the discharge port. Averaged over the last calculated male rotor revolution, the mass flow is $0.146\ \text{kg/s}$ which equals an inlet volume flow of $0.126\ \text{m}^3/\text{s}$. The theoretical volume flow rate, derived from chamber volumes and rotational speed, is $0.177\ \text{m}^3/\text{s}$, i. e. volume efficiency is 71.1%. The averaged power within the same interval is 24.1 kW. The time resolved values for mass flow are shown in Figure 17.

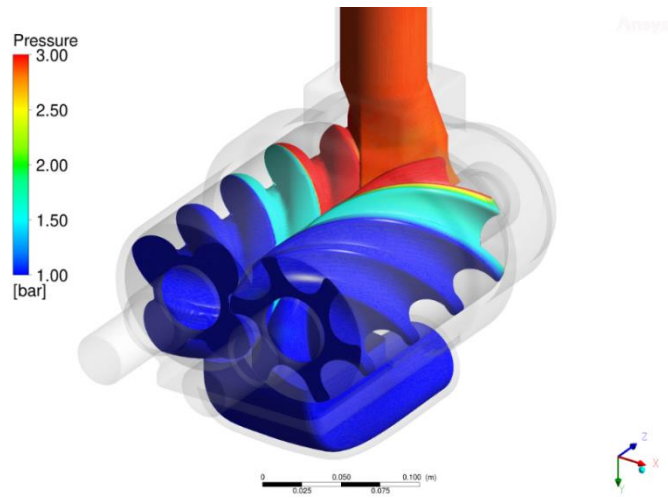


Figure 7: Absolute pressure (initial geometry)

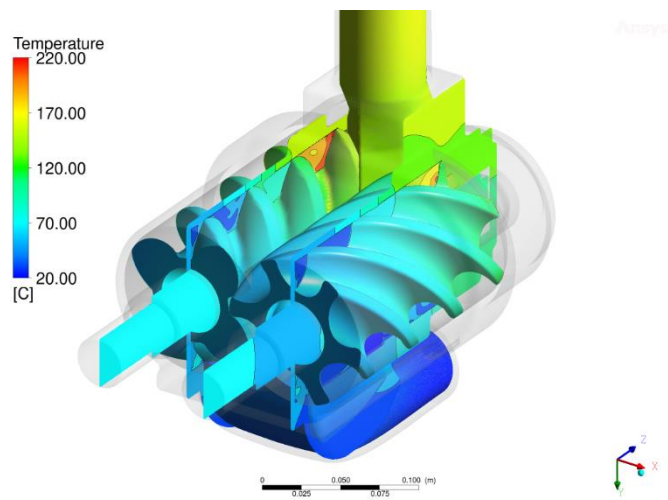


Figure 8: Temperature (initial geometry)

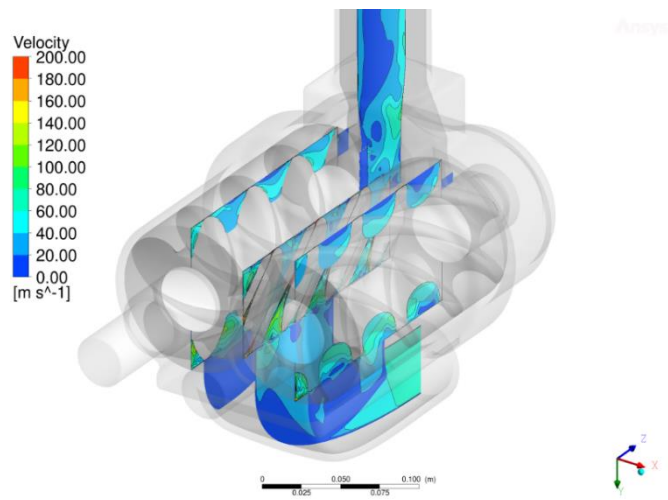


Figure 9: Velocity (initial geometry)

4.2. Structural results

For the structural results the deformations and therefore changes in radial and axial clearance are of most interest. Figure 10 shows the scaled deformation of the rotors. Because of the increasing temperature towards the discharge port the outer diameter of the rotors is also increasing. The housing is deformed more at the top side (discharge pipe), because a frictionless support is used on the bottom side and the temperature at the outlet pipe is much higher, see Figure 11.

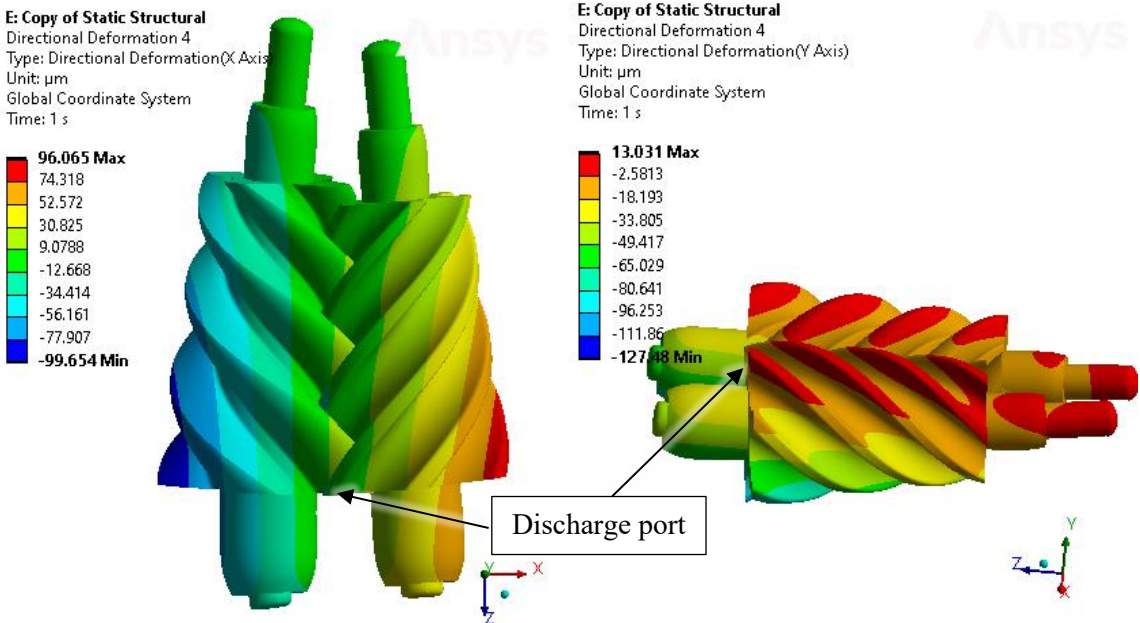


Figure 10: Rotor deformation scaled by a factor of 250 (left: x-deformation, right: y-deformation)

The deformation of both rotor shafts and the housing comes mainly from the temperature gradients inside the bodies. The structural results could be used to adapt the flow volume depending on the deformation of the rotors and the casing. In comparison to the whole model, the deformation is small but it has a large influence on the flow through the clearances.

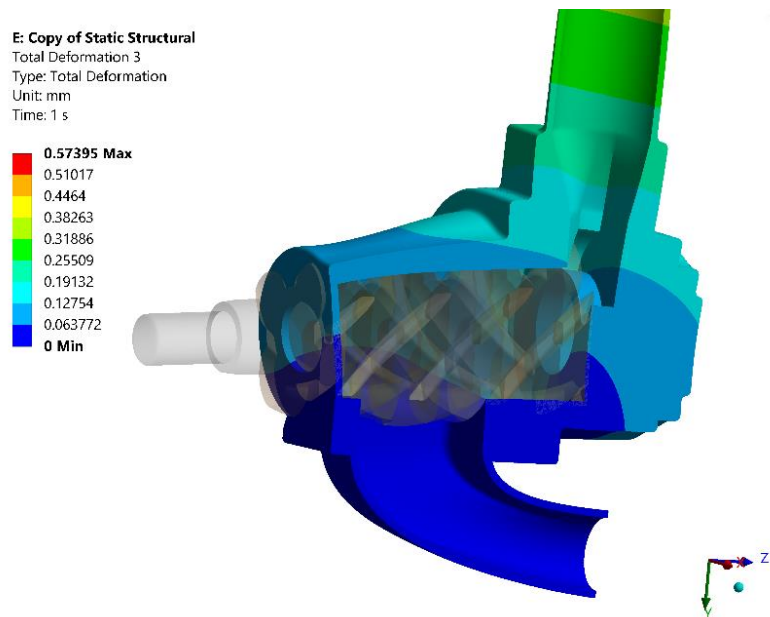


Figure 11: Casing deformation scaled by a factor of 250

4.3. Transferring clearance changes into CFD geometry

TwinMesh has the possibility to modify the radial clearance size depending on the position along the rotor axis by bending and scaling of the rotors. TwinMesh does not support housing deformation yet, this will be included in the next release. Depending on the deformations calculates by the structural solver, it may not possible to reach the exact deformation by using the available options.

To get a simplified definition paths are created for each rotor in x and y-direction, see Figure 12. Along these paths the deformation values are exported for the rotors and the casing. For missing values in between, where no solid is located along the path, the values are linearly interpolated.

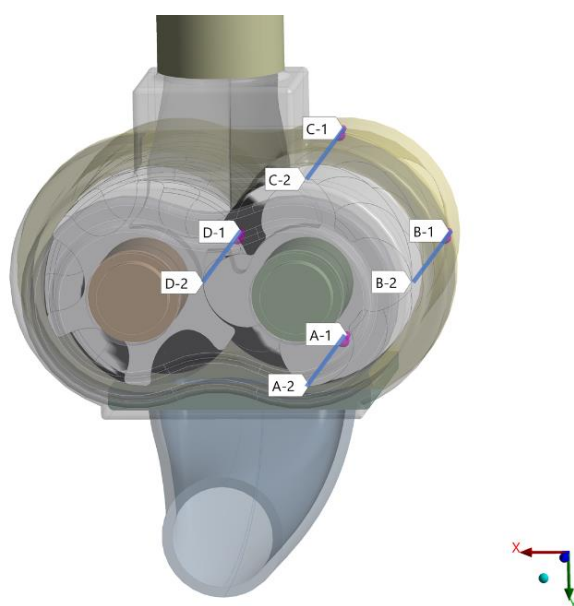


Figure 12: Paths to get deformation values for the main rotor

The variation of clearance size can be calculated from the deformation values, called “target” values here. Figure 13 (dashed lines) shows that the intermesh clearance and the clearance in positive y-direction is decreasing towards the discharge port depending on the increasing rotor (mainly thermal deformation). On the negative y-direction the clearance increases because the deformation of the casing is larger than the thermal expansion of the rotor. On the female rotor the same tendency exists (Figure 14).

The modified radial clearances could be realized in TwinMesh by specifying the axis position and the scaling offset (positive value means a shrinking rotor normal to the rotor surface) depending on the position along the rotor axis, see Figure 15 and Figure 16. In addition to that the casing radius is reduced along the x-axis by 50 μm (slightly oval curvature).

Figure 13 and Figure 14 show the realized deformations (solid lines). The intermesh clearance and the radial clearances in y-direction are good in comparison to the structural results (dashed lines). Only the x-direction gap to the casing is different.

The change of the axial clearance is not taken into account in the following CFD simulation because only a constant axial clearance size could be defined in TwinMesh for both rotors. The axial clearance for male rotor on the suction side changes from 100 μm to 46 μm and on the pressure side to 107 μm, for the female rotor on the suction side from 100 μm to 71 μm and on the pressure side to 106 μm.

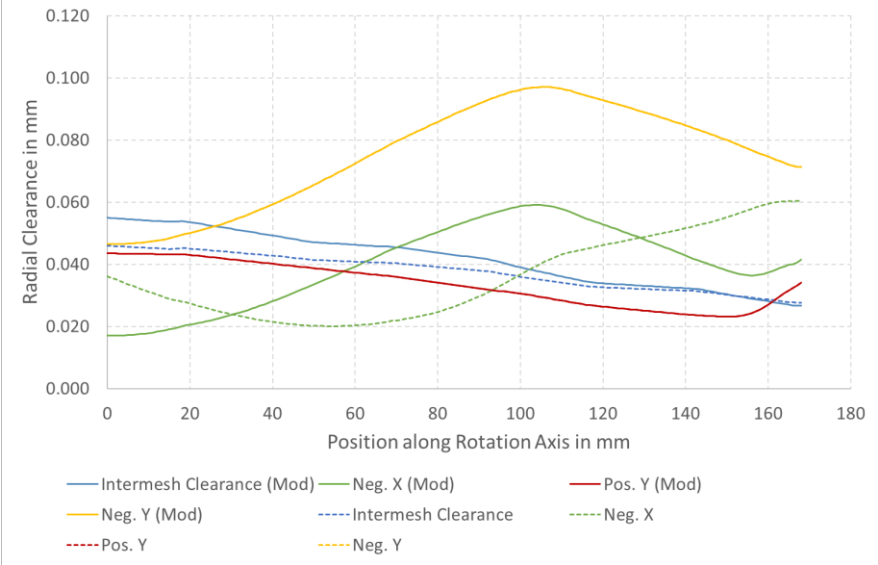


Figure 13: Target (dashed) and realized (solid) radial clearances of the male rotor

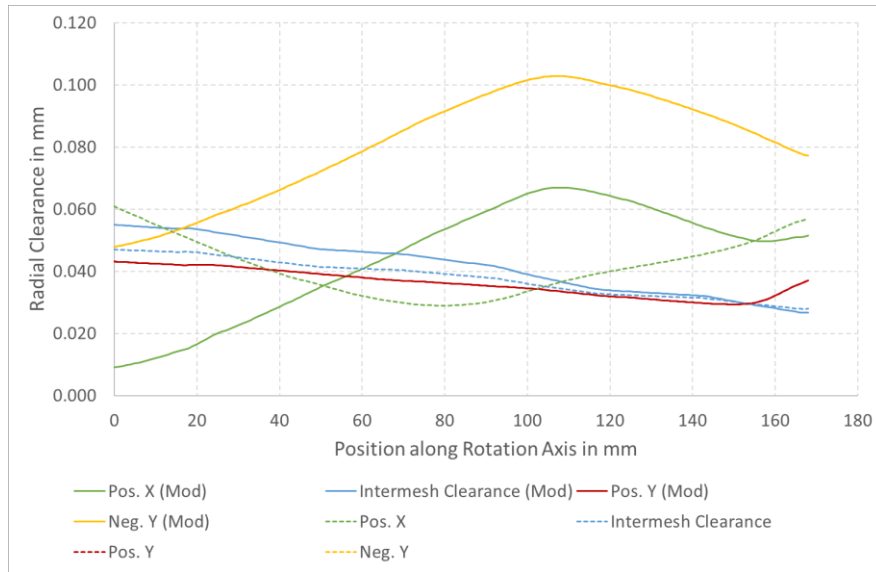


Figure 14: Target (dashed) and realized (solid) radial clearances of the female rotor

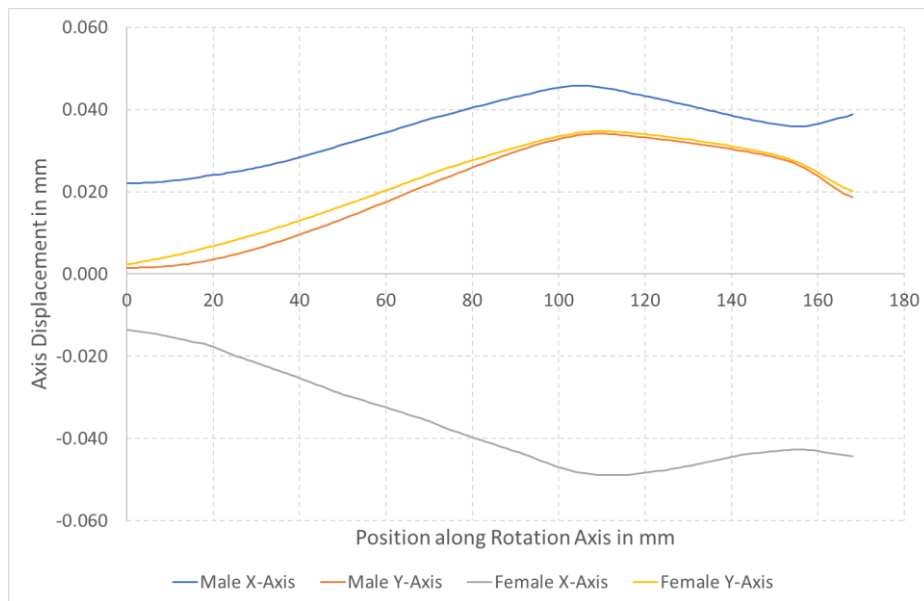


Figure 15: Axis displacement

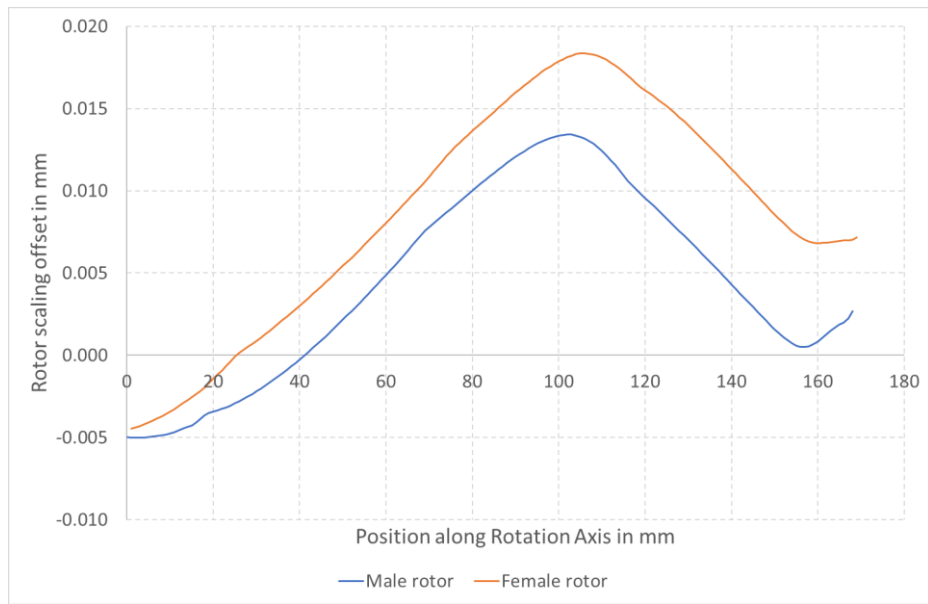


Figure 16: Rotor scale offset

4.4. CFD results for adapted geometry

The flow field looks nearly the same as without modified clearances. The influence of modified clearances (mainly reduced clearance size) can be seen by the mass flow and the power. As expected, mass flow and the power increase after adapting deformation. The mass flow is now 0.151 kg/s (+2.9%) and the power 24.7 kW (+2.5%). The volume efficiency rises to 73.1%.

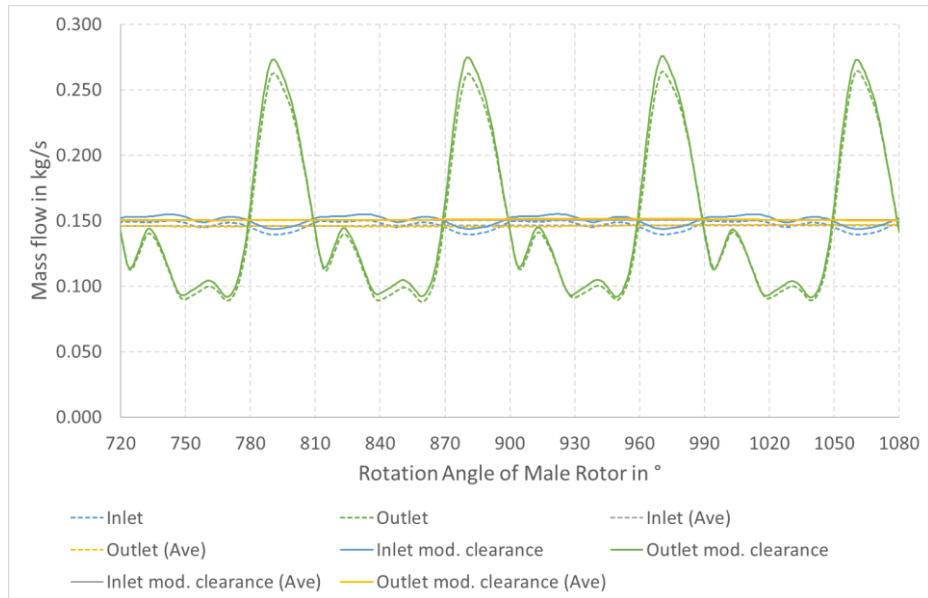


Figure 17: Mass flow for initial (dashed) and adapted (solid) geometry over rotation angle

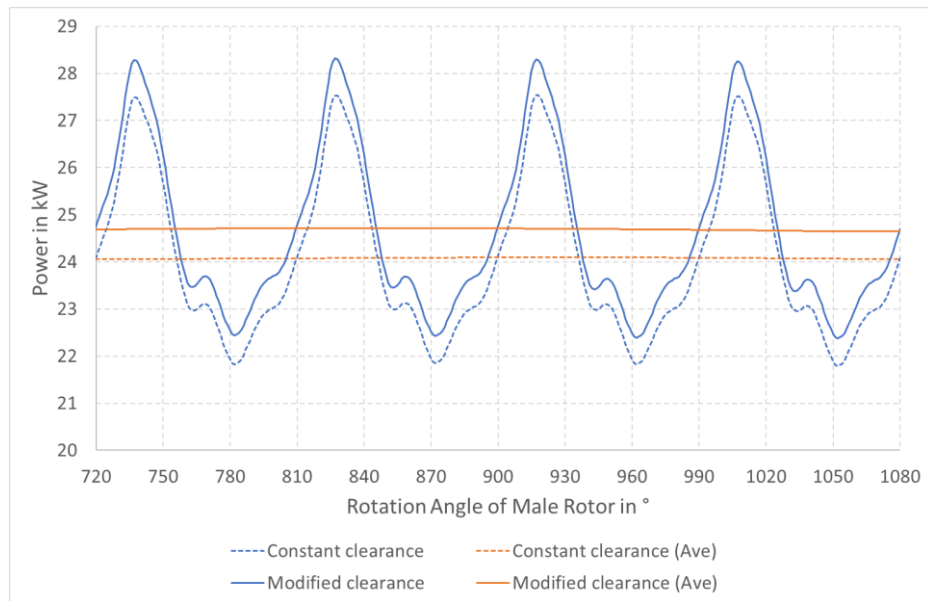


Figure 18: Power for initial (dashed) and adapted (solid) geometry over rotation angle

5. Summary and outlook

This paper shows one workflow to adapt the deformation results of a structural simulation to a CFD setup. It starts with a CFD simulation (including CHT for the rotor and housing solids) with constant radial clearances using TwinMesh to realize the necessary mesh deformation inside the working chamber and Ansys CFX as the CFD solver. In a next step the temperature of the housing and the rotor solids and the pressure on the fluid sides are mapped on a structural mechanical setup solved by Ansys Mechanical. The change of the radial clearances depending on the deformation of the solids is used as an input for the final CFD simulation using an adapted mesh for the working chambers.

A simplified method to take the change of the radial clearance sizes along the rotor axis into account was shown. It can be used to see the impact on the machine behaviour in more detail and get more realistic results for the real operating condition.

The next step will be to develop a direct method to modify the mesh of the working chambers for each location (radial and axial clearances) depending in the structural deformation values. The challenge is to keep the mesh quality high by considering all degrees of freedom of the deformation.

References

- [1] Nikolov A., Huck C., Brümmer A. (2012). Influence of Thermal Deformation on the Characteristic Diagram of a Screw Expander in Automotive Application of Exhaust Heat Recovery. 21st International Compressor Engineering Conference, Purdue
- [2] Buckney D., Kovacevic A., Stosic N. (2014). Accounting for Local Therman Distortions in a Chamber Model for Twin Screw Compressors. 22nd International Compressor Engineering Conference, Purdue
- [3] Kovacevic A., Stosic N., Smith I. (2007). Screw compressors: three dimensional computational fluid dynamics and solid fluid interaction vol 46 (Springer Science & Business Media)
- [4] Spille-Kohoff, A., Hesse J., El Shorbagy A. (2015). CFD simulation of a screw compressor including leakage flows and rotor heating. 9 th International conference on compressors and their systems (ICCS), London
- [5] Andres, R., Hesse, J., Low, D. (2018). CFD Simulation Of A Two Stage Twin Screw Compressor Including Leakage Flows And Comparison With Experimental Data. 24th International Compressor Engineering Conference, Purdue

- [6] Wu, H., Huang, H., Zhang, B., Xiong, B., Lin, K. (2019). CFD Simulation and Experimental Study of Working Process of Screw Refrigeration Compressor with R134a. *Energies* Vol. 12 (issue 11)
- [7] Andres, R., Hesse, J., Salecker, U., Spille-Kohoff, A., Nikolov, A., Brümmer, A. (2016). CFD Simulation of a Twin Screw Expander including Leakage Flows, 23rd International Compressor Engineering Conference, Purdue
- [8] Horst Stöcker (1998). *Taschenbuch der Physik*, Verlag Harri Deutsch, p. 691.